chemosensors

Article

Simplified Synthesis of Blue Light-Emitting CdSe/ZnS Core–Shell Quantum Dots

Yi-Zhi Lin, Sheng-Tong Wu, Zi-Chen Pan and Shou-Nian Ding *

Jiangsu Province Hi-Tech Key Laboratory for Bio-Medical Research, School of Chemistry and Chemical Engineering, Southeast University, Nanjing 211189, China; lin_yizhi@seu.edu.cn (Y.-Z.L.); 230228796@seu.edu.cn (S.-T.W.); 230249832@seu.edu.cn (Z.-C.P.)

* Correspondence: snding@seu.edu.cn; Fax: +86-25-52090621

Abstract

Blue-emitting CdSe/ZnS quantum dots require precise control of crystal growth because variations in particle size and surface structure can strongly influence their emission properties. In this study, blue-optical CdSe/ZnS core–shell quantum dots were synthesized using a one-step hot-injection method. Structural and optical characterization confirmed the formation of crystalline QDs with stable fluorescence emission after ZnS shell coating. The synthesized QDs exhibited an average diameter of approximately 3 nm, blue emission at 461 nm, and a photoluminescence quantum yield of 93.31%. The QDs exhibited suitable optical properties for fluorescence-based bioanalytical applications for HCG.

Keywords: quantum dots; hot-injection; blue QDs; burst nucleation; high-performance; LFA

1. Introduction

Quantum dots (QDs) belong to semiconductor nanocrystals with characteristic diameters falling between 2 and 10 nm (CdSe QDs normally comprising approximately 10^2 to 10^5 atoms) [1–4]. When the physical sizes of these particles are below the exciton Bohr radius of the bulk substance, QDs demonstrate noticeable quantum confinement effects. This restricts the movement of charge carriers (electrons and holes) in three dimensions, resulting in discrete, atom-like energy levels [3]. A distinguishing feature of QDs is their size-adjustable photoluminescence: as the size of the nanocrystal grows, the emission wavelength undergoes a red shift because of the narrowing of the bandgap. Furthermore, QDs are identified to possess exceptionally high photoluminescence quantum yields (PLQY), wide excitation spectra, and sharp emission profiles in contrast to conventional organic fluorophores, greatly surpassing traditional organic fluorescent markers in terms of brightness and color purity [1]. Recent advances in nanomaterial engineering have further expanded the usage scope of fluorescent probes in lateral flow assays (LFA) by improving signal amplification and quantitative detection capability [5].

Controlling nucleation and growth is essential for obtaining QDs with narrow size distributions and stable emission properties, but this control can be difficult to maintain in simplified synthesis procedures. Achieving uniform particle sizes requires precise control of reaction kinetics [2]. In the strong confinement regime, a 1 nm change in diameter can shift the emission wavelength by 20–30 nm, requiring millisecond-level control of reaction quenching [6,7]. Surface dangling bonds can also act as nonradiative recombination centers. Inorganic shells such as ZnS passivate the core, but the approximately 12% lattice mismatch between CdSe and ZnS can introduce interfacial strain and defects [8,9]. Intermediate

Check for updates

Received: 14 August 2026
Revised: 19 September 2026
Accepted: 21 September 2026
Published: 24 September 2026

Copyright: © 2026 by the authors. Licensee MDPI, Basel, Switzerland. This article is an open access article distributed under the terms and conditions of the Creative Commons Attribution (CC BY) license.

layers, such as ZnSe, are often used to reduce this strain. Material selection also involves a trade-off between optical performance and toxicity. Although Cd-based QDs offer high optical performance, Cd-free alternatives such as InP can have lower PLQYs (<80%) [10,11] and limited operational stability, including T80 lifetimes below 100 h in certain perovskite-enhanced systems [12,13]. Scale-up is further constrained by inefficient micromixing in large reactors, where Reynolds numbers below 1000 can broaden the particle size distribution, and by purification costs [14]. The cost of medical-grade QDs can exceed USD 5000 per gram because of the complexity of ligand exchange and bioconjugation.

The fabrication of blue-emitting CdSe quantum dots has long presented a substantial technical barrier for synthetic researchers, as the diminutive dimensions of such particles necessitate stringent regulation of both nucleation and growth procedures [15–18], with additional shifts toward the violet region of the electromagnetic spectrum resulting in pronounced surface lability and uncontrollable kinetic behavior during particle formation. When the particle diameter approaches the exciton Bohr radius, minor fluctuations within nucleation and growth environments are capable of exerting a notable influence on both the light-emitting wavelength and the photoluminescence quantum yield of the final products. It has been identified by researchers that even tiny deviations from optimized reaction parameters during the preparation process can lead to substantial deviations in the optoelectronic properties of these small-sized light-emitting nanomaterials, as the high surface energy associated with ultra-small quantum dot structures often drives undesired particle aggregation and defect generation that directly undermine emission performance.

While individual QDs hold outstanding photophysical characteristics, their direct utilization as fluorescent labels in lateral flow assays is frequently constrained. The inadequate signal generation, complex surface functionalization, and diminished colloidal stability throughout biological manipulation restrict the unmodified employment of such particles. To overcome these limitations, QDs-embedded polymer microspheres have been fabricated as advanced fluorescent reporting elements by incorporating large quantities of QDs into a single polymer matrix [19,20]. This architectural setup facilitates the transformation of multiple nanoscale light emitters into a unified signal-amplification module. The unit enhances detection because the immunorecognition event generates fluorescence from hundreds to thousands of QDs rather than a single fluorophore. The module boosts the detection performance since the occurrence of immunorecognition yields fluorescence from hundreds to thousands of QDs instead of a lone fluorophore. As a result, LFAs built on QD-incorporated polymer microspheres display markedly elevated signal strength and refined analytical detection sensitivity when juxtaposed with traditional single-QD probes [21]. For instance, polymer-derived QD nanobead labeling agents have been effectively adopted in sandwich-format LFAs, attaining roughly one order of magnitude enhancement in analytical detection sensitivity as opposed to conventional nanoparticle-dependent assays. Recent investigations further revealed that fine-tuned QD nanobeads can deliver more intense fluorescence emission while sustaining appropriate particle sizes for smooth migration across nitrocellulose membranes, permitting quantitative measurement with optimized limits of detection [20–22].

Apart from the magnification of detection signals, embedding QDs within a polymer matrix furnishes extra merits regarding photophysical robustness and the performance of colloidal systems. As a substantial proportion of atoms resides on the exterior of nanocrystals, discrete QDs exhibit pronounced susceptibility to the oxidation of surfaces, the detachment of ligand molecules, and fluctuations in surrounding conditions. The encapsulation of QDs within polymer microspheres achieves physical separation of QDs from external surroundings and mitigates the deterioration of fluorescence intensity throughout the periods of storage and experimental procedure execution. Moreover, the polymer

framework impedes direct contact between adjacent QDs, suppressing the fluorescence quenching effect dependent on concentration that arises from Förster resonance energy transfer (FRET) or aggregation-induced nonradiative recombination. Therefore, the spatial arrangement pattern of QDs within polymer carriers plays a pivotal role in striking a balance between elevated loading of fluorophores and the efficacy of fluorescence emission. Existing scholarly inquiries have highlighted that minuscule fluorescent microspheres embedded with highly dispersed QDs offer a viable methodological approach to attaining robust fluorescence signals without compromising the stability of colloids or the assay reproducibility [20,22,23].

CdSe is one of the most extensively studied materials for colloidal quantum dots because its optical properties can be tuned through nanocrystal size. As the particle size decreases into the quantum-confined regime, the electronic states become increasingly confined and the effective band gap increases, resulting in a shift in the absorption and emission toward shorter wavelengths [24]. This size dependence is particularly relevant to blue-emitting CdSe quantum dots, which generally require very small cores to achieve sufficient quantum confinement.

The preparation of such small nanocrystals, however, is often accompanied by a stronger influence of the surface. Their large surface-to-volume ratio increases the contribution of under-coordinated atoms and surface defect states, which can act as carrier traps and promote nonradiative recombination [25]. Surface passivation is therefore important for maintaining efficient photoluminescence in small CdSe nanocrystals. A common approach is to grow a wider-bandgap semiconductor shell around the CdSe core. In CdSe/ZnS quantum dots, the ZnS shell reduces the influence of surface defects, improves the confinement of photogenerated carriers, and protects the emissive core from degradation. As a result, the core–shell structure combines the size-dependent optical properties of CdSe with improved photoluminescence efficiency and stability provided by the ZnS shell [26].

Another important advantage of QD-embedded microspheres is the outstanding surface functionalization potential for the coupling of biomolecules. In contrast to individual QDs, whose tiny dimension restricts the quantity of available functional groups and may undermine antibody orientation post-modification. At the present stage, the polymer microspheres that can be procured generally already possess pre-functionalized surfaces. This permits the efficient immobilization of antibodies while sustaining antigen-binding activity and boosting the stability of biological conjugates in the process of lateral flow migration [27]. The elevated particle size also aids interaction with capture molecules on the test line, elevating the possibility of successful sandwich complex formation. Consequently, LFAs based on QD nanobeads have revealed enhanced detection performance for diverse biological markers, encompassing viral antibodies and protein targets [19,28,29].

In the present investigation, a streamlined single-step hot-injection protocol was utilized for the fabrication of blue-emitting CdSe/ZnS core–shell quantum dots. Through precise adjustment of the reactivity of precursors and the ratios of ligand to metal, we have initiated a “burst nucleation” event that disentangles the nucleation and growth stages [30–32]. The optimized approach streamlines the operation process and alleviates the uncontrolled growth of ultrasmall quantum dots (reducing Ostwald ripening effects on emission). It provides a more attainable and replicable pathway for the manufacturing of large batches. The obtained QDs were afterwards embedded into polymer microspheres and assessed as fluorescent labels for LFA.

2. Materials and Methods

2.1. Reagents

Cadmium oxide (CdO, 99.5%), zinc acetate ($Zn(CH_3COO)_2$, 99.9%), selenium powder (Se, 99.9%), sulfur powder (S, 99.99%), oleic acid (OA, 90%), 1-octadecene (ODE, 90%), trioctylphosphine (TOP, 97%), and n-hydroxysuccinimide (NHS, 97%) were purchased from Sigma-Aldrich (St. Louis, MO, USA). Acetone, 2-Morpholinoethanesulphonic acid (MES), Tween-20, toluene, diethyl ether, n-hexane, ethanol and chloroform (trichloromethane, analytical grade) were obtained from Sinopharm Chemical Reagent Co., Ltd. (Shanghai, China). EDC was purchased from Energy Chemical Co. LTD. (Shanghai, China); BSA purchased from Shanghai Aladdin Biochemical Technology Co., Ltd. (Shagnhai, China); HCG antibody and antigen, Goat Anti-mouse Immunoglobulin G (IgG), Sample Pad, NC Film, Absorbent Pad, and Polyvinyl Chloride (PVC) Substrate purchased from Shanghai Jieyi Biotechnology Co., LTD. (Shanghai, China).

2.2. Testing Instrument

Electronic analytical balance (BSA224S-CW, Sartorius, Göttingen, Germany); Transmission electron microscope (TECNAI G2 20, FEI Company, Hillsboro, OR, USA); High-resolution transmission electron microscope (Talos P200X G2, Thermo Fisher SCIENTIFIC, Hillsboro, OR, USA); Fluorescence spectrophotometer (RF-6000, Shimadzu Corporation, Kyoto, Japan); UV–Vis spectrophotometer (UV2600, Shimadzu Corporation, Kyoto, Japan); Particle size and zeta potential analyzer (Marvern Zetasizer, Nano ZS, Worcestershire, UK); Steady-state transient fluorescence spectrometer (Edinburgh Instruments FLS1000, Edinburgh Instruments, Livingston, UK).

2.3. Synthesis of QDs

This paper synthesizes hydrophobic CdSe/ZnS QDs modified from the reported "one-step synthesis method" [33]. First, 0.1 mmol cadmium oxide, 4.3 mmol zinc acetate, 5 mL OA, and 15 mL ODE were added to a 250 mL four-neck round-bottom flask. The mixture was heated to 150 °C under magnetic stirring and nitrogen protection and maintained for 30 min. Subsequently, after heating the mixture to 310 °C, a pre-mixed solution containing 0.1 mmol Se, 4.3 mmol S, and 3 mL TOP was rapidly injected into the flask via syringe and held at 300 °C for 10 s. The reaction flask was then rapidly cooled to room temperature using cold air. Finally, the reacted mixture was purified by sequential washing with toluene and acetone, followed by centrifugation at 10,000 rpm. This washing-centrifugation cycle was repeated three times. The resulting product was dissolved in toluene or chloroform to obtain purified CdSe/ZnS QDs.

2.4. Synthesis of Quantum Dots-Doped Particles (QPs)

50 μL PS-COOH solution was washed and resuspended in 0.8 mL of butanol three times. Then, 100 μL QDs (in hexane) and 100 μL of PS-COOH (in hexane) were mixed and dropped into the vigorously stirred PS-COOH suspension. The mixtures were stirred for 30 min at room temperature and sonicated three times (1 min) every 10 min until the QDs had penetrated the particles. The prepared QPs were purified by washing four times with 50% ethanol, and then suspended in 10% ethanol solution. The QPs were suspended at 5 mg/mL in 10% ethyl alcohol solution at 4 °C.

2.5. Antibody Conjugation Protocol

The swelling-treated carboxylated microspheres were covalently conjugated to antibodies using a standard two-step EDC/NHS coupling procedure. Briefly, the microspheres were washed and equilibrated in 50 mM MES buffer (pH 6.0), followed by surface acti-

vation using a mixture of EDC and NHS (or Sulfo-NHS) for 30 min at room temperature under gentle agitation. After activation, the unreacted crosslinkers were rapidly removed by centrifugation, and the microspheres were immediately resuspended in 10 mM PBS buffer (pH 7.4) containing the target antibody. The mixture was incubated for 2 h at room temperature (or overnight at 4 °C) to facilitate covalent amide bond formation between the activated carboxyl groups and the primary amines of the antibody. Subsequently, the remaining active sites on the microsphere surface were blocked with a blocking buffer (containing 1% BSA) for 60 min to minimize non-specific binding. Finally, the antibody-conjugated microspheres were washed three times via centrifugation and stored in a PBS storage buffer containing 0.1% BSA at 4 °C for further applications.

2.6. Fabrication of the LFA Test Strip

The sample pad was cut into 12 mm-wide strips, soaked in a PBS solution (pH 7.4, 0.01 M) containing 2% NaCl, 0.1% Tween-20, 1% saccharose and 1% polyvinylpyrrolidone 55K, and then dried at 37 °C. The test (T) line was prepared by uniformly dispensing HCG-β antibody (2 mg mL^{-1}) onto the NC membrane, while the control (C) line was generated by dispensing diluted IgG (2 mg mL^{-1}) onto the same membrane. The coated NC membrane was dried under room temperature. Subsequently, the PVC backing card, NC membrane, pretreated sample pad, and absorbent pad were assembled sequentially. After the NC membrane was fixed at the center of the PVC substrate, the sample pad and absorbent pad were attached to both ends of the substrate, respectively. An overlap of approximately 1–2 mm was maintained between the NC membrane and the sample/absorbent pads to ensure continuous liquid migration. Finally, the assembled strips were cut into 3 mm-wide test strips using a strip cutter and stored at 4 °C for further use.

2.7. Detection of HCG with LFA Test Strips

For quantitative detection, QP-ABs conjugates dispersed in 0.01 M PBS were mixed with recombinant HCG antigen solutions at a series of concentrations. The mixtures were subsequently applied to the pretreated sample pads of the test strips. After allowing sufficient reaction and migration for approximately 25 min, the fluorescence intensity of the test strips was recorded using a dry fluorescence immunoassay analyzer (DFIA).

3. Results

As illustrated in Figure 1, the blue CdSe/ZnS core–shell quantum dots (BQDs) exhibit a relatively uniform particle size. Specifically, the TEM micrograph shown in Figure 1A appears consistent and homogeneous. Meanwhile, Figure 1B reveals an average particle size of approximately 3 nm, presenting some degree of size variation. Clear lattice fringes were observed in Figure 1C, with most of the measured d-spacings falling between 0.31 and 0.32 nm. The average value was 0.316 ± 0.007 nm, close to the (111) spacing of cubic ZnS (~0.312 nm). A similar value of 0.317 nm has been reported for thick-shell CdSe/ZnS QDs [34]. Due to the extremely small ratio of the added amounts of Cd and Se, the CdSe core is relatively small, while a much larger fraction of the final particle is occupied by the ZnS-rich outer layer. The lattice fringes resolved from the whole particle are therefore mainly associated with the ZnS lattice, making the smaller CdSe contribution difficult to distinguish directly from the HRTEM images. However, Cd and Se signals remained detectable in Figure 1D together with Zn and S, which is consistent with the retention of the CdSe core after shell growth. Thus, the HRTEM results mainly reflect the ZnS-rich outer region, while the EDS results provide complementary compositional evidence for the CdSe component within the particles.

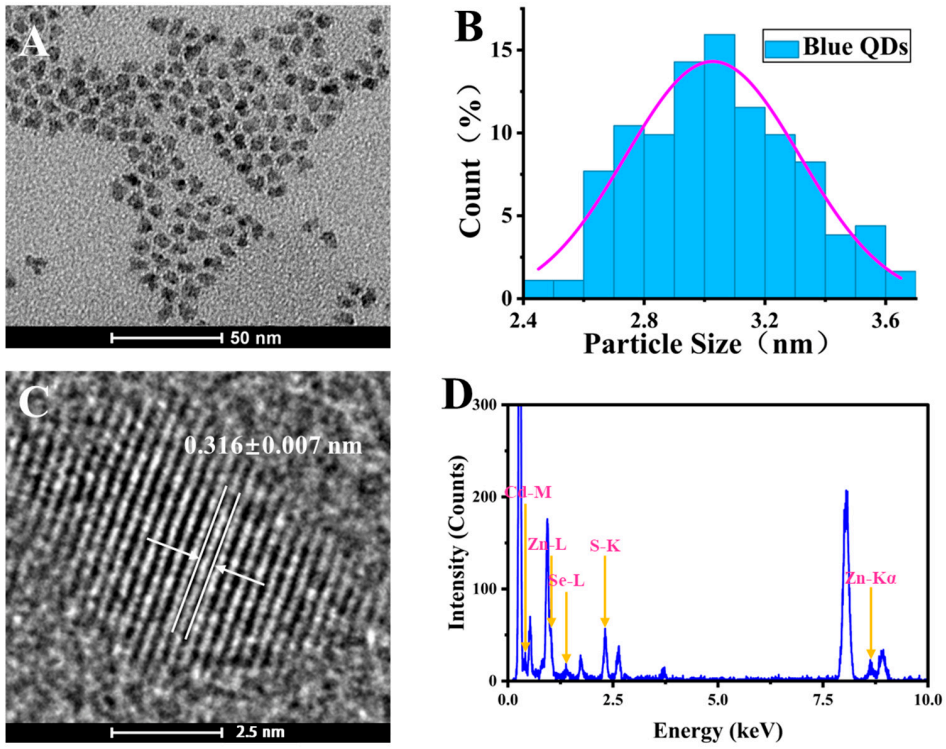


Figure 1. Structural characterization of blue-emitting CdSe/ZnS quantum dots (BQDs). (**A**) Transmission electron microscopy (TEM) image; (**B**) particle size distribution; (**C**) high-resolution TEM image showing the lattice spacing; and (**D**) energy-dispersive X-ray spectroscopy (EDS) spectrum.

As depicted in Figure 2A, the QDs exhibit their strongest excitation wavelength at 300 nm, yet demonstrate a characteristically broad excitation bandwidth, enabling activation across a wide spectral range. Notably, under these broad excitation conditions, the emission wavelength maintains remarkable stability with a well-defined peak at 461 nm.

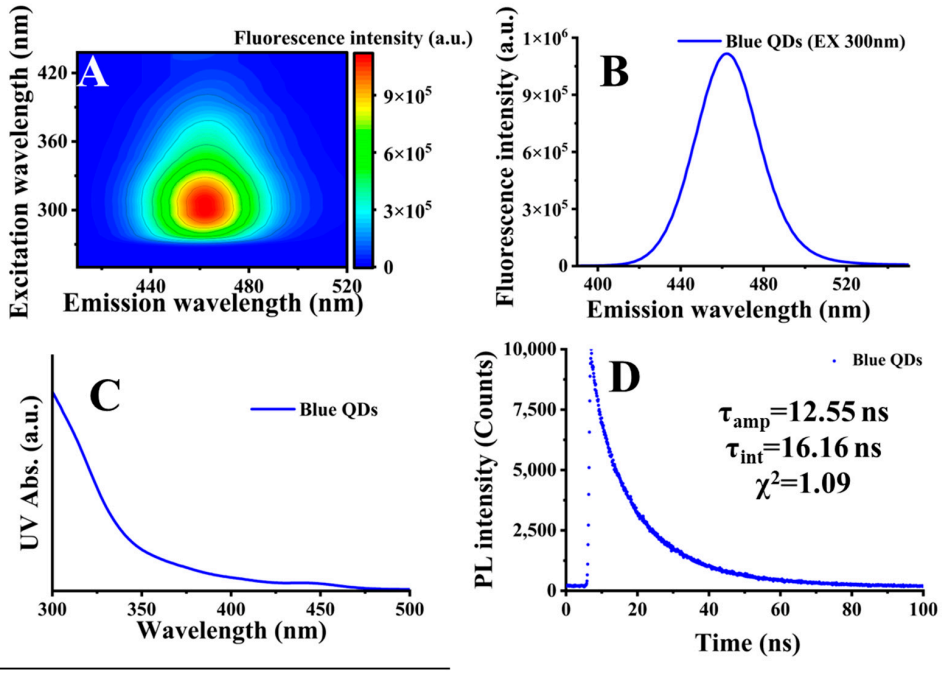


Figure 2. (**A**) 3D fluorescence spectrum of BQDs; (**B**) fluorescence emission spectrum at the 300 nm excitation wavelength of BQDs; (**C**) ultraviolet absorption map of BQDs; (**D**) fluorescence lifetime test spectrum of BQDs.

However, the emission spectrum in Figure 2B shows a moderate FWHM of approximately 35 nm. The relatively broad emission band may be associated with the limited size control inherent to the simplified synthesis and the sensitivity of ultrasmall QDs to slight variations during nucleation and growth. Because the growth period is extremely short at such small particle sizes, small differences in nucleation time can translate into appreciable variations in particle size. In addition, the high surface-to-volume ratio of ultrasmall QDs makes the formation of uniform surface states more difficult. These factors may increase the contribution of surface traps, resulting in a broader emission band and lower fluorescence intensity. Figure 2C shows a weak absorption feature in the 430–445 nm range, which can be attributed to the CdSe core. As shown in Figure 2D, the average fluorescence lifetime is approximately 16 ns. This relatively short lifetime can be related to the direct-bandgap nature of CdSe (~1.74 eV), which favors rapid radiative recombination. The lifetime is therefore shorter than that reported for PbS QDs (200–800 ns) but longer than that of perovskite QDs (1–15 ns). The strong quantum confinement in these small QDs may further affect the radiative recombination dynamics. Meanwhile, the ZnS shell helps passivate surface defects and suppress nonradiative recombination, thereby improving the fluorescence efficiency.

The as-synthesized CdSe/ZnS QDs showed a high PLQY of 93.31% (±2.48%), with the emission peak centered at 461 nm. The PLQY was measured five times using a relative method, with a 0.1 M quinine sulfate solution used as the standard. The UV–vis spectrum exhibited relatively weak absorption in the 430–445 nm region, resulting in a noticeable separation between the absorption and emission features. The fluorescence decay was measured by time-correlated single-photon counting and analyzed using a multi-exponential decay model, following commonly used procedures for CdSe/ZnS QDs [35,36]. The fitted decay gave an average fluorescence lifetime of approximately 16 ns, with a reduced chi-square value (χ^2) of 1.09. A reduced χ^2 value close to unity indicates satisfactory agreement between the fitted function and the experimental decay data. Together, these optical characteristics are consistent with effective surface passivation of the QDs. The relatively large spectral separation between excitation and emission may further reduce spectral overlap and, consequently, self-absorption. TEM images showed slightly irregular particle contours, which may be associated with the inorganic shell-growth process during surface passivation.

4. Discussion

Obtaining blue-optical CdSe/ZnS quantum dots requires careful control of the CdSe core size. Smaller CdSe cores exhibit stronger quantum confinement, which generally leads to emission at shorter wavelengths. In the present synthesis, the core growth time is particularly important because the CdSe cores are formed within a relatively short reaction period. Small variations in this period can therefore cause changes in particle size and emission wavelength.

The synthesis used in this work was adapted from a previously reported one-step method, with modifications to the temperature control during CdSe core growth. Because the reaction rate is strongly affected by temperature, the reaction mixture was cooled rapidly after nucleation by lowering the ambient temperature and increasing air convection. This reduced the cooling time (about 10 min) available for further growth of the CdSe cores and helped limit their final size. The smaller core size then resulted in a shift in the emission toward shorter wavelengths. In this way, the reported synthesis procedure was modified to improve control over the short growth period required for the preparation of blue-emitting CdSe/ZnS QDs.

The nucleation and subsequent growth of colloidal quantum dots largely determine their final structural and optical properties during hot-injection synthesis. These processes can be described by the LaMer-Dinegar model [30,37–40]. Under appropriate reaction conditions, rapid precursor conversion leads to a short nucleation period, after which crystal growth proceeds as the precursor concentration decreases. Consequently, controlling the relative rates of nucleation and growth is important for achieving a desired particle size distribution and optical performance [41].

A simplified synthetic strategy was developed by controlling the precursor composition, ligand coordination, and reaction duration. In this procedure, CdSe core formation and ZnS shell growth were carried out within a single reaction process, allowing blue-emitting CdSe/ZnS core–shell quantum dots to be obtained [42]. Compared with conventional multistep synthesis, the simplified procedure reduces experimental complexity while retaining high fluorescence efficiency.

The large surface-to-volume ratio of ultrasmall nanocrystals makes the synthesis of blue-emitting CdSe/ZnS quantum dots particularly sensitive to reaction kinetics [14,15]. Even small changes in precursor conversion, ligand binding, or surface reconstruction can affect surface defect formation and, consequently, the optical properties of the resulting QDs [43]. For this reason, careful control of the surface chemistry throughout the synthesis is important to promote efficient radiative recombination.

The interface between the CdSe core and ZnS shell is not necessarily compositionally abrupt. Previous studies have shown that CdSe/ZnS quantum dots can contain an alloyed interfacial region, which has been attributed to CdSe dissolution and redistribution of the constituent elements during shell growth. In the present synthesis, the Se- and S-containing precursors are introduced within the same injection step, allowing CdSe formation and Zn/S precursor conversion to occur within an overlapping reaction period. This difference in precursor addition may promote greater intermixing at the core–shell interface and result in a relatively broad transition region between the CdSe-rich core and ZnS-rich outer region. Thus, the shell is more appropriately considered a ZnS-rich layer with an interfacial Cd–Zn–Se–S region rather than an ideally sharp compositional boundary [33,44]. However, based on previous studies, we found that due to the significant difference in the input ratio, the outer layer encapsulation of ZnS exhibited pure crystal spacings. Such interfacial alloying is compatible with a core–shell architecture and may arise from the reaction kinetics during the growth process.

During crystal growth, oleic acid and trioctylphosphine act as ligands that coordinate with the precursors and help stabilize the nanocrystal surface. Changes in the ligand environment can also affect surface reconstruction and defect formation, which in turn influences the emission efficiency of the QDs [41,45,46]. Appropriate ligand coordination helps suppress particle aggregation and excessive growth, favoring the formation of QDs with a relatively narrow size distribution. Once the desired degree of growth has been reached, prompt termination of the reaction helps retain the intended particle size and optical properties.

The formation of the ZnS shell provides additional passivation of the CdSe core. By reducing surface trap states and suppressing non-radiative recombination pathways, shell growth can improve the photoluminescence efficiency of CdSe-based QDs. Previous studies have shown that appropriate shell structures and surface passivation are important for improving the PLQY of semiconductor nanocrystals [8,9,47]. However, excessive shell growth may introduce interfacial strain and defects. Therefore, the shell thickness and growth conditions should be carefully controlled to balance effective surface passivation with favorable optical properties.

The synthesized QDs had an average diameter of approximately 3 nm and showed blue emission centered at 461 nm, with a PLQY of 93.31%. Such a high PLQY is consistent with effective surface passivation during synthesis, in agreement with previous reports indicating that suppression of surface defects is important for improving the PLQY of QDs [47]. The relatively broad emission bandwidth may be associated with the size distribution and surface heterogeneity of these ultrasmall QDs. Despite this spectral broadening, the strong fluorescence intensity and stable optical properties support their use as fluorescent labels in polymer microsphere-based biosensing systems.

Table 1 summarizes previously reported approaches for the synthesis of CdSe/ZnS and related blue-emitting quantum dots. Dabbousi et al. established an important foundation for core–shell passivation across the visible spectral range, although the reported PLQYs were relatively low (30–50%) and the stability of blue-emitting QDs remained limited [1]. Čapek et al. subsequently achieved precise size control in the range of 1.5–2.2 nm and improved the safety of the synthesis by using zinc carboxylates. However, their hot-injection method required stringent control of nucleation kinetics, which can make reproducible synthesis more challenging, while the resulting emission peak at 475 nm was still relatively long for deep-blue emission [48]. Ou et al. developed a Cd-free core–shell system with blue emission near 450 nm and a narrow FWHM of approximately 24 nm through an environmentally benign synthetic strategy [49]. The PLQY of the QDs, however, was limited to 44%. Compared with these reported systems, the QDs obtained in the present work combine a relatively simple synthesis with a higher PLQY, highlighting their potential for applications requiring efficient blue fluorescence.

Table 1. Comparison of selected blue core–shell quantum dots.

	This Work	**Early Foundation [1]**	**Blue Emission Optimization [48]**	**Cd-Free System [49]**
Materials	CdSe/ZnS	CdSe/ZnS	CdSe/ZnS	$CuGaS_2$/GaS/ZnS
Synthesis method	Simplified one-step hot injection	Traditional hot injection	Prefocused hot injection	Intermediate layer auxiliary hot injection
Emission wavelength	461 nm	470–625 nm	475 nm	Near 450 nm
PLQY	93.31%	30–50%	40–50%	44%
FWHM	~35 nm	≤40 nm	Not reported	24 nm

Using the synthesized QDs, blue QD-incorporated PS-COOH fluorescent particles were prepared through a swelling-based encapsulation strategy. The resulting fluorescent particles were subsequently functionalized to obtain QP-ABs, which were used as fluorescent labels for the detection of human chorionic gonadotropin (HCG).

Previous work has suggested that sufficient spatial separation between neighboring QDs can reduce the probability of FRET and thus limit fluorescence quenching [50]. As shown in Figure 3B, the surface charge of the fluorescent microspheres was further examined by zeta potential measurements. Before antibody conjugation, the microspheres exhibited a negative zeta potential. Following conjugation, the absolute value of the negative zeta potential decreased, supporting the successful immobilization of antibodies on the microsphere surface. The resulting antibody-functionalized fluorescent microspheres were therefore suitable for subsequent sandwich immunochromatographic assays, as shown in Figure 3A. Their quantitative detection performance was evaluated using DFIA. Antigen solutions at different concentrations were tested, and the corresponding fluorescence intensities were recorded. As shown in Figure 3C, the fluorescence signal increased linearly with antigen concentration, indicating a reliable quantitative response. Linear regression

yielded an LOD of 1.34 ng/mL. The coefficient of variation in the same batch of test strips for the HCG concentration of 1 μg/mL, 100 ng/mL and 10 ng/mL in three consecutive tests was 0.58%, 1.17% and 1.52%. The selectivity of the test strip was confirmed by detecting four different antigens (HCG, AFP, CEA and CA125) of 1 μg/mL and using a blank PBS.

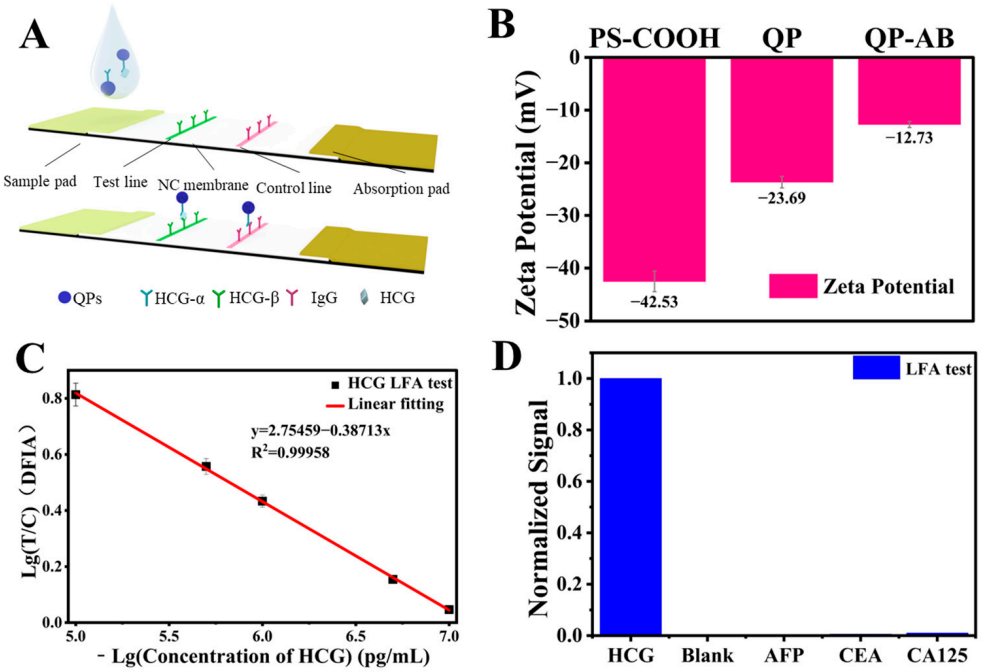


Figure 3. (**A**) LFA test illustration. (**B**) Zeta Potential of PS-COOH, QPs and QP-Abs. (**C**) Linear fitting of the LFA test strip results. (**D**) Selectivity of LFA test strips.

However, Cd-based QDs, such as CdSe/ZnS, have been widely used in fluorescence-based biosensing because of their high photoluminescence efficiency, narrow emission bands, broad excitation ranges, and good photostability. These properties are particularly useful when a strong fluorescence signal or multiplexed detection is required [51]. However, the presence of cadmium limits their use in biological applications. Cd^{2+} can be released when the QD surface or shell is degraded, and both released cadmium ions and the physicochemical properties of the nanoparticles can contribute to cytotoxicity [52]. ZnS shell coating can reduce Cd leakage and improve the stability of the QDs, although it does not completely remove the potential risk associated with cadmium-containing materials [53].

Cd-free QDs, including InP- and $CuInS_2$-based QDs, have therefore been investigated as alternatives for biological applications. Their main advantage is the avoidance of cadmium-related toxicity, while recent developments have improved their fluorescence efficiency and surface modification [54]. However, some Cd-free QDs still show broader emission bands, and their synthesis, surface chemistry, and colloidal stability can be more difficult to control than those of established Cd-based QDs. Thus, Cd-based QDs still provide useful optical performance for sensitive in vitro biosensing, although their potential Cd leakage and associated biosafety concerns should be considered when evaluating their suitability for biological applications.

5. Conclusions

In conclusion, this work reports a straightforward yet robust method for the synthesis of high-quality blue CdSe/ZnS core–shell QDs. The reaction conditions provided effective control over crystal growth and surface passivation. The synthesized blue CdSe/ZnS QDs exhibit favorable optical properties, suggesting potential for future applications in

biosensing and optoelectronics. The synthesized QDs were subsequently incorporated into polymer microspheres and applied as fluorescent labels in a lateral flow assay for the detection of human chorionic gonadotropin (HCG). These results demonstrate the potential of the developed CdSe/ZnS QD-based fluorescent probes for sensitive biosensing applications.

Author Contributions: Conceptualization, Y.-Z.L. and S.-N.D.; methodology, Y.-Z.L., S.-T.W. and Z.-C.P.; formal analysis, Y.-Z.L.; investigation, Y.-Z.L. and Z.-C.P.; resources, S.-N.D.; data curation, Y.-Z.L. and S.-T.W.; writing—original draft preparation, Y.-Z.L. and Z.-C.P.; writing—review and editing, Y.-Z.L., S.-T.W. and S.-N.D.; visualization, Y.-Z.L.; supervision, S.-N.D.; project administration, S.-N.D.; funding acquisition, S.-N.D.; All authors have read and agreed to the published version of the manuscript.

Funding: This research was funded by the National Natural Science Foundation of China, grant number 22574020.

Institutional Review Board Statement: Not applicable.

Informed Consent Statement: Not applicable.

Data Availability Statement: The data presented in this study are available on request from the corresponding author.

Conflicts of Interest: The authors declare no conflicts of interest.

Abbreviations

The following abbreviations are used in this manuscript:

QDs	Quantum dots
BQDs	Blue-emitting quantum dots
FRET	Förster resonance energy transfer
PLQY	Photoluminescence quantum yield
FWHM	Full width at half maximum
LFA	Lateral flow assay
QPs	QD-loaded polymer particles
QP-ABs	Antibody-conjugated QD-loaded polymer particles
LOD	Limit of detection
HCG	Human chorionic gonadotropin
PS-COOH	Carboxylated polystyrene
DFIA	Dry fluorescence immunoassay analyzer
TEM	Transmission electron microscopy
HRTEM	High-resolution transmission electron microscopy
EDS	Energy-dispersive X-ray spectroscopy
NC	Nitrocellulose
PBS	Phosphate-buffered saline
BSA	Bovine serum albumin

References

1. Dabbousi, B.O.; Rodriguez-Viejo, J.; Mikulec, F.V.; Heine, J.R.; Mattoussi, H.; Ober, R.; Jensen, K.F.; Bawendi, M.G. (CdSe)ZnS Core−Shell Quantum Dots: Synthesis and Characterization of a Size Series of Highly Luminescent Nanocrystallites. *J. Phys. Chem. B* **1997**, *101*, 9463–9475. [CrossRef]
2. Murray, C.B.; Norris, D.J.; Bawendi, M.G. Synthesis and Characterization of Nearly Monodisperse Cde (E = Sulfur, Selenium, Tellurium) Semiconductor Nanocrystallites. *J. Am. Chem. Soc.* **1993**, *115*, 8706–8715. [CrossRef]
3. Brus, L.E. Electron–Electron and Electron-Hole Interactions in Small Semiconductor Crystallites: The Size Dependence of the Lowest Excited Electronic State. *J. Chem. Phys.* **1984**, *80*, 4403–4409. [CrossRef]
4. Li, X.; Du, J.; Guo, J.; Wu, K. Colloidal Quantum Dot Liquid Lasers. *Adv. Mater.* **2026**, *38*, e18662. [CrossRef]

5. Sena-Torralba, A.; Álvarez-Diduk, R.; Parolo, C.; Piper, A.; Merkoçi, A. Toward Next Generation Lateral Flow Assays: Integration of Nanomaterials. *Chem. Rev.* **2022**, *122*, 14881–14910. [CrossRef]
6. Efros, A.L.; Efros, A.L. Interband Absorption of Light in a Semiconductor Sphere. *Sov. Phys. Semicond.-Ussr* **1982**, *16*, 772–775.
7. Weller, H. Colloidal Semiconductor Q-Particles: Chemistry in the Transition Region Between Solid State and Molecules. *Angew. Chem. Int. Ed. Engl.* **1993**, *32*, 41–53. [CrossRef]
8. Hines, M.A.; Guyot-Sionnest, P. Synthesis and Characterization of Strongly Luminescing ZnS-Capped CdSe Nanocrystals. *J. Phys. Chem.* **1996**, *100*, 468–471. [CrossRef]
9. Xie, R.; Kolb, U.; Li, J.; Basché, T.; Mews, A. Synthesis and Characterization of Highly Luminescent CdSe−Core CdS/$Zn_{0.5}Cd_{0.5}S$/ZnS Multishell Nanocrystals. *J. Am. Chem. Soc.* **2005**, *127*, 7480–7488. [CrossRef]
10. Jang, E.; Kim, Y.; Won, Y.H.; Jang, H.; Choi, S.M. Environmentally Friendly Inp-Based Quantum Dots for Efficient Wide Color Gamut Displays. *ACS Energy Lett.* **2020**, *5*, 1316–1327. [CrossRef]
11. Stam, M.; Almeida, G.; Ubbink, R.F.; van der Poll, L.M.; Vogel, Y.B.; Chen, H.; Giordano, L.; Schiettecatte, P.; Hens, Z.; Houtepen, A.J. Near-Unity Photoluminescence Quantum Yield of Core-Only Inp Quantum Dots via a Simple Postsynthetic Inf3 Treatment. *ACS Nano* **2024**, *18*, 14685–14695. [CrossRef]
12. Won, Y.-H.; Cho, O.; Kim, T.; Chung, D.-Y.; Kim, T.; Chung, H.; Jang, H.; Lee, J.; Kim, D.; Jang, E. Highly Efficient and Stable Inp/ZnSe/ZnS Quantum Dot Light-Emitting Diodes. *Nature* **2019**, *575*, 634–638. [CrossRef]
13. Kim, J.S.; Heo, J.-M.; Park, G.-S.; Woo, S.-J.; Cho, C.; Yun, H.J.; Kim, D.-H.; Park, J.; Lee, S.-C.; Park, S.-H.; et al. Ultra-Bright, Efficient and Stable Perovskite Light-Emitting Diodes. *Nature* **2022**, *611*, 688–694. [CrossRef]
14. Marre, S.; Jensen, K.F. Synthesis of Micro and Nanostructures in Microfluidic Systems. *Chem. Soc. Rev.* **2010**, *39*, 1183–1202. [CrossRef]
15. Talapin, D.V.; Rogach, A.L.; Haase, M.; Weller, H. Evolution of an Ensemble of Nanoparticles in a Colloidal Solution: Theoretical Study. *J. Phys. Chem. B* **2001**, *105*, 12278–12285. [CrossRef]
16. Qu, L.H.; Peng, X.G. Control of Photoluminescence Properties of CdSe Nanocrystals in Growth. *J. Am. Chem. Soc.* **2002**, *124*, 2049–2055. [CrossRef]
17. Tao, C.-L.; Ma, J.; Wei, C.; Xu, D.; Xie, Z.; Jiang, Z.; Ge, F.; Zhang, H.; Xie, M.; Ye, Z.; et al. Scalable Synthesis of High-Quality Core/Shell Quantum Dots with Suppressed Blinking. *Adv. Opt. Mater.* **2023**, *11*, 2300533. [CrossRef]
18. Zhang, J.; Li, C.; Li, J.; Peng, X. Synthesis of CdSe/ZnSe Core/Shell and CdSe/ZnSe/ZnS Core/Shell/Shell Nanocrystals: Surface-Ligand Strain and CdSe–ZnSe Lattice Strain. *Chem. Mater.* **2023**, *35*, 7049–7059. [CrossRef]
19. Zhou, Y.; Chen, Y.; Liu, W.; Fang, H.; Li, X.; Hou, L.; Liu, Y.; Lai, W.; Huang, X.; Xiong, Y. Development of a Rapid and Sensitive Quantum Dot Nanobead-Based Double-Antigen Sandwich Lateral Flow Immunoassay and Its Clinical Performance for the Detection of Sars-Cov-2 Total Antibodies. *Sens. Actuators B Chem.* **2021**, *343*, 130139. [CrossRef]
20. Li, X.; Yan, W.; Wang, Y.; Yu, R.-J.; Han, H.; Zhang, P. Plasmon-Enhanced Quantum Dot Nanobead-Based Lateral Flow Assay with Lower Background and Improved Sensitivity. *ACS Appl. Nano Mater.* **2025**, *8*, 4120–4128. [CrossRef]
21. Tang, X.; Xia, W.; Han, H.; Wang, Y.; Wang, B.; Gao, S.; Zhang, P. Dual-Fluorescent Quantum Dot Nanobead-Based Lateral Flow Immunoassay for Simultaneous Detection of C-Reactive Protein and Procalcitonin. *ACS Appl. Bio Mater.* **2024**, *7*, 7659–7665. [CrossRef]
22. Yan, W.; Xia, W.; Hu, Q.; Zeng, S.; Han, H.; Zhang, P. Digital Counting of Quantum Dots Nanobeads on Lateral Flow Test Strips Enables Ultrasensitive Point-of-Care Diagnostics. *Anal. Chem.* **2026**, *98*, 13546–13555. [CrossRef]
23. Chen, X.; Zheng, Q.; Li, X.; Wang, L.; Zhang, L.; Zhang, Y.; Wang, L.; Lv, Y.; Li, L.S.; Wu, R. One-Pot Fabrication of Highly Stable and Luminescent Inp Quantum Dots Nanobeads through Multifunctional Polymer Encapsulation for Lateral Flow Immunoassay. *Anal. Chim. Acta* **2026**, *1383*, 344924. [CrossRef]
24. Bai, R.; Wang, C.; Ramzan, M.; Chang, S.; Zhong, H. Progress in Blue Colloidal Quantum Dots for Display Applications. *J. Inf. Disp.* **2025**, *26*, 95–107. [CrossRef]
25. Li, S.N.; Pan, J.L.; Yu, Y.J.; Zhao, F.; Wang, Y.K.; Liao, L.S. Advances in Solution-Processed Blue Quantum Dot Light-Emitting Diodes. *Nanomaterials* **2023**, *13*, 1695. [CrossRef]
26. Wang, X.; Wang, P.; Li, M.; Li, J. Advances in the Preparation and Biological Applications of Core@Shell Nanocrystals Based on Quantum Dots and Noble Metal. *RSC Adv.* **2024**, *14*, 26308–26324. [CrossRef]
27. Lin, T.; Huang, X.; Guo, L.; Zhou, S.; Li, X.; Liu, Y.; Hu, J.; Chen, X.; Xiong, Y. Boronate Affinity-Assisted Oriented Antibody Conjugation on Quantum Dot Nanobeads for Improved Detection Performance in Lateral Flow Immunoassay. *Microchem. J.* **2021**, *171*, 106822. [CrossRef]
28. Qi, H.; Sun, Q.; Ma, Y.; Wu, P.; Wang, J. Advantages of Lateral Flow Assays Based on Fluorescent Submicrospheres and Quantum Dots for Clostridium Difficile Toxin B Detection. *Toxins* **2020**, *12*, 722. [CrossRef]
29. Zhang, Y.; Lv, Y.; Chen, X.; Ye, Y.; Yu, S.; Li, N.; Yao, H.; Wang, Z.; Feng, Q.; Wu, R.; et al. Ultrasensitive Point-of-Care Multiplex Diagnosis for Influenza Virus Based Robust Quantum Dot Microsphere-Lateral Flow Immunoassay. *Biosens. Bioelectron.* **2025**, *273*, 117187. [CrossRef]

30. LaMer, V.K.; Dinegar, R.H. Theory, Production and Mechanism of Formation of Monodispersed Hydrosols. *J. Am. Chem. Soc.* **1950**, *72*, 4847–4854. [CrossRef]
31. Park, J.; Joo, J.; Kwon, S.G.; Jang, Y.; Hyeon, T. Synthesis of Monodisperse Spherical Nanocrystals. *Angew. Chem. Int. Ed.* **2007**, *46*, 4630–4660. [CrossRef]
32. Hendricks, M.P.; Campos, M.P.; Cleveland, G.T.; Plante, I.J.-L.; Owen, J.S. A Tunable Library of Substituted Thiourea Precursors to Metal Sulfide Nanocrystals. *Science* **2015**, *348*, 1226–1230. [CrossRef]
33. Bae, W.K.; Char, K.; Hur, H.; Lee, S. Single-Step Synthesis of Quantum Dots with Chemical Composition Gradients. *Chem. Mater.* **2008**, *20*, 531–539. [CrossRef]
34. Hao, J.; Liu, H.; Miao, J.; Lu, R.; Zhou, Z.; Zhao, B.; Xie, B.; Cheng, J.; Wang, K.; Delville, M.-H. A Facile Route to Synthesize CdSe/ZnS Thick-Shell Quantum Dots with Precisely Controlled Green Emission Properties: Towards Qds Based Led Applications. *Sci. Rep.* **2019**, *9*, 12048. [CrossRef]
35. Xu, H.; Chmyrov, V.; Widengren, J.; Brismar, H.; Fu, Y. Mechanisms of Fluorescence Decays of Colloidal CdSe–Cds/ZnS Quantum Dots Unraveled by Time-Resolved Fluorescence Measurement. *Phys. Chem. Chem. Phys.* **2015**, *17*, 27588–27595. [CrossRef]
36. Acharjee, D.; Kanti Panda, M.; Baran Mahato, A.; Das, A.; Ghosh, S. Evidence of Carrier Diffusion Between Emission States in CdSe/ZnS Core–Shell Quantum Dots: A Comprehensive Investigation Combining Fluorescence Lifetime Correlation Spectroscopy (Flcs) and Single Dot Photoluminescence Studies. *Nanoscale* **2024**, *16*, 18444–18454. [CrossRef]
37. Kwon, S.G.; Hyeon, T. Formation Mechanisms of Uniform Nanocrystals Via Hot-Injection and Heat-up Methods. *Small* **2011**, *7*, 2685–2702. [CrossRef]
38. Vreeland, E.C.; Watt, J.; Schober, G.B.; Hance, B.G.; Austin, M.J.; Price, A.D.; Fellows, B.D.; Monson, T.C.; Hudak, N.S.; Maldonado-Camargo, L.; et al. Enhanced Nanoparticle Size Control by Extending Lamer's Mechanism. *Chem. Mater.* **2015**, *27*, 6059–6066. [CrossRef]
39. Whitehead, C.B.; Özkar, S.; Finke, R.G. Lamer's 1950 Model for Particle Formation of Instantaneous Nucleation and Diffusion-Controlled Growth: A Historical Look at the Model's Origins, Assumptions, Equations, and Underlying Sulfur Sol Formation Kinetics Data. *Chem. Mater.* **2019**, *31*, 7116–7132. [CrossRef]
40. Zhang, F.; Shang, L.; Zhang, Z.; Cheng, Y.; Liu, H.; Du, X. Controllable Synthesis of Metal Nanoparticles under Non-Equilibrium Conditions Via an Extended Lamer Mechanism. *Small Methods* **2026**, *10*, e02275. [CrossRef]
41. Du, L.; Arabzadeh Nosratabad, N.; Jin, Z.; Zhang, C.; Wang, S.; Chen, B.; Mattoussi, H. Luminescent Quantum Dots Stabilized by N-Heterocyclic Carbene Polymer Ligands. *J. Am. Chem. Soc.* **2021**, *143*, 1873–1884. [CrossRef]
42. Karmakar, S.; Kanti Das, T.; Kalarikkal, N.; Saha, A. A Simplified Approach for the Aqueous Synthesis of Luminescent CdSe/ZnS Core/Shell Quantum Dots and Their Applications in Ultrasensitive Determination of the Biomarker 3-Nitro-L-Tyrosine. *Langmuir* **2022**, *38*, 15995–16003. [CrossRef]
43. Sahu, A.; Kumar, D. Core-Shell Quantum Dots: A Review on Classification, Materials, Application, and Theoretical Modeling. *J. Alloys Compd.* **2022**, *924*, 166508. [CrossRef]
44. Fernández-Delgado, N.; Herrera, M.; Tavabi, A.H.; Luysberg, M.; Dunin-Borkowski, R.E.; Rodriguez-Cantó, P.J.; Abargues, R.; Martínez-Pastor, J.P.; Molina, S.I. Structural and Chemical Characterization of CdSe-ZnS Core-Shell Quantum Dots. *Appl. Surf. Sci.* **2018**, *457*, 93–97. [CrossRef]
45. Yin, Y.; Alivisatos, A.P. Colloidal Nanocrystal Synthesis and the Organic–Inorganic Interface. *Nature* **2005**, *437*, 664–670. [CrossRef]
46. Kilina, S.V.; Tamukong, P.K.; Kilin, D.S. Surface Chemistry of Semiconducting Quantum Dots: Theoretical Perspectives. *Acc. Chem. Res.* **2016**, *49*, 2127–2135. [CrossRef]
47. Xiao, P.; Zhang, Z.; Ge, J.; Deng, Y.; Chen, X.; Zhang, J.-R.; Deng, Z.; Kambe, Y.; Talapin, D.V.; Wang, Y. Surface Passivation of Intensely Luminescent All-Inorganic Nanocrystals and Their Direct Optical Patterning. *Nat. Commun.* **2023**, *14*, 49. [CrossRef]
48. Čapek, R.K.; Lambert, K.; Dorfs, D.; Smet, P.F.; Poelman, D.; Eychmüller, A.; Hens, Z. Synthesis of Extremely Small CdSe and Bright Blue Luminescent CdSe/ZnS Nanoparticles by a Prefocused Hot-Injection Approach. *Chem. Mater.* **2009**, *21*, 1743–1749. [CrossRef]
49. Ou, K.; Zheng, J.; Zhao, J.; Wang, K.; Qin, X.; Yang, W.; Du, Z.; Fu, H. Unlocking High-Efficiency Narrow-Band Blue Emission: Gas Interlayer Design in Eco-Friendly Cugas2 Quantum Dots as a Superior Alternative. *ACS Appl. Nano Mater.* **2026**, *9*, 5769–5778. [CrossRef]
50. Bradley, M.; Bruno, N.; Vincent, B. Distribution of CdSe Quantum Dots within Swollen Polystyrene Microgel Particles Using Confocal Microscopy. *Langmuir* **2005**, *21*, 2750–2753. [CrossRef]
51. Quesada-González, D.; Merkoçi, A. Quantum Dots for Biosensing: Classification and Applications. *Biosens. Bioelectron.* **2025**, *273*, 117180. [CrossRef]
52. Wang, Y.; Pang, S.; Chen, Z.; Wang, J.; Liu, L.; Zhang, L.; Wang, F.; Song, M. Surface Modification Determines the Distribution and Toxicity of Quantum Dots During the Development of Early Staged Zebrafish. *Environ. Sci. Technol.* **2023**, *57*, 10574–10581. [CrossRef]

53. Lin, X.; Chen, T. A Review of in Vivo Toxicity of Quantum Dots in Animal Models. *Int. J. Nanomed.* **2023**, *18*, 8143–8168. [CrossRef]
54. Son, Y.; Kim, Y.J.; Han, D.G.; Eom, T.; Kim, D.; Kim, N.; Park, M. Red/Nir-Emissive, Cadmium-Free Quantum Dots: Synthesis, Luminescence Mechanisms, and Applications. *Sensors* **2026**, *26*, 2473. [CrossRef]

Disclaimer/Publisher's Note: The statements, opinions and data contained in all publications are solely those of the individual author(s) and contributor(s) and not of MDPI and/or the editor(s). MDPI and/or the editor(s) disclaim responsibility for any injury to people or property resulting from any ideas, methods, instructions or products referred to in the content.